ACS NANO

Cite This: ACS Nano 2019, 13, 9048−9056

www.acsnano.org

ARTICLE

Defect-Tolerant Plasmonic Elliptical Resonators for Long-Range Energy Transfer

Felipe V. Antolinez,[†] Jan M. Winkler,[†] Patrik Rohner,[‡] Stephan J. P. Kress,[†] Robert C. Keitel,[†] David K. Kim,[†] Patricia Marqués-Gallego,[†] Jian Cui,[†,§] Freddy T. Rabouw,[†,⊥] Dimos Poulikakos,[‡] and David J. Norris*[,†]

[†]Optical Materials Engineering Laboratory, Department of Mechanical and Process Engineering, ETH Zurich, 8092 Zurich, Switzerland

[‡]Laboratory of Thermodynamics in Emerging Technologies, Department of Mechanical and Process Engineering, ETH Zurich, 8092 Zurich, Switzerland

Supporting Information

ABSTRACT: **Energy transfer allows energy to be moved from one quantum emitter to another. If this process follows the Förster mechanism, efficient transfer requires the emitters to be extremely close (<10 nm). To increase the transfer range, nanophotonic structures have been explored for photon- or plasmon-mediated energy transfer. Here, we fabricate high-quality silver plasmonic resonators to examine long-distance plasmon-mediated energy transfer. Specifically, we design elliptical resonators that allow energy transfer between the foci, which are separated by up to 10 μm. The geometry of the ellipse guarantees that all plasmons emitted from one focus are collected and channeled through different paths to the other focus. Thus, energy can be transferred even if a micrometer-sized defect obstructs the direct path between the focal points. We characterize the spectral and spatial profiles of the resonator modes and show that these can be used to transfer energy between green- and red-emitting colloidal quantum dots printed with subwavelength accuracy using electrohydrodynamic nanodripping. Rate-equation modeling of the time-resolved fluorescence from the quantum dots further confirms the long-distance energy transfer.**

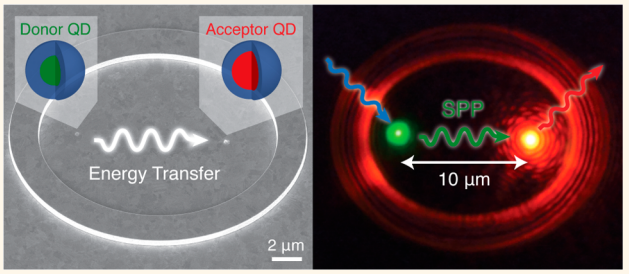

KEYWORDS: *energy transfer, colloidal quantum dots, surface plasmon polaritons, elliptical resonator, plasmonics, electrohydrodynamic printing*

Förster energy transfer allows an electronic excitation to move from one quantum emitter (the "donor") to another (the "acceptor").[1,2] The excitation is transferred directly through dipole−dipole interactions, without emission of a photon. The efficiency of this process depends on the intensity of the electric near-field that the donor generates at the acceptor. For two dipoles in a homogeneous medium, the transfer rate scales as $1/r^6$, where r is the donor−acceptor separation. Thus, this process is efficient only for small separations (r < 10 nm).[3] To transfer energy between quantum emitters over longer distances, which can be desirable for quantum technologies,[4−6] the emitters must interact *via* the lower-intensity far-field components of the electric field. This far-field interaction can be seen as radiative energy transfer from donors to acceptors *via* photons.

Nanophotonic structures can be useful for achieving long-distance energy transfer. For example, such structures can be designed to increase the electric-field intensity from the donor at the position of the acceptor.[7−9] In photon-mediated energy transfer, the field must be effectively channeled to, and collected by, the acceptor. Optical microcavities[10,11] or metamaterials[12] have been shown to enhance energy transfer for distances up to 160 nm. For even longer distances, dielectric waveguides can direct photons from a source to a receiver with low loss but have limited coupling efficiencies for nanoscale emitters due to their size mismatch with the diffraction-limited optical mode.[13,14]

Plasmonic structures offer another approach.[15,16] Metal−dielectric interfaces support surface plasmon polaritons (SPPs), which are electromagnetic waves coupled to charge-density oscillations. These waves can guide energy along a surface.[17] Due to the confinement of the plasmon field to the interface, SPPs can couple to quantum emitters more efficiently than photons can in dielectric structures.[18,19] Indeed, it has been shown that a flat Ag−dielectric interface mediates energy transfer from a donor to an acceptor

Received: April 25, 2019
Accepted: July 11, 2019
Published: July 11, 2019

DOI: 10.1021/acsnano.9b03201
ACS Nano 2019, 13, 9048−9056

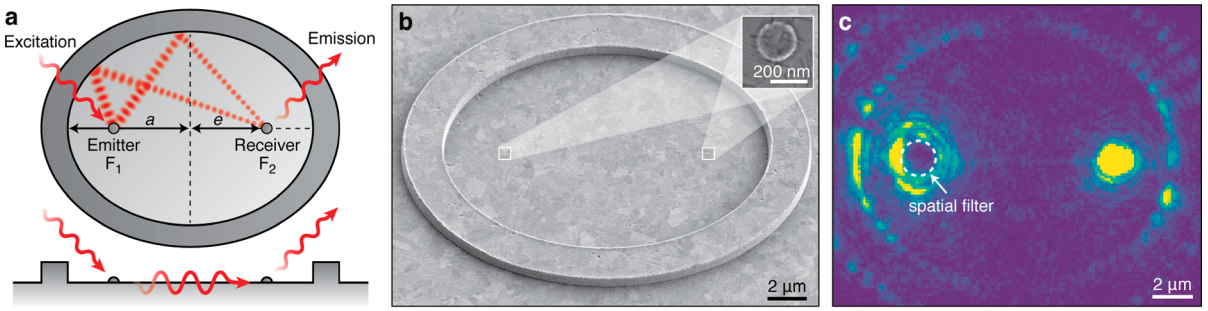

Figure 1. Properties of the plasmonic elliptical resonator. (a) Schematic of the elliptical resonator. The emitter (donor) and receiver (acceptor) are placed at the foci F_1 and F_2, respectively, and are separated by 2*e*. All SPPs launched from F_1 propagate 2*a* and undergo one reflection before arriving at F_2 (except for SPPs propagating on the direct path between F_1 and F_2). (b) Scanning electron micrograph (SEM) of a template-stripped Ag elliptical resonator with 2*a* = 16 μm and 2*e* = 10 μm; the reflector height is ∼600 nm. Ag disks are placed at the two focal points and act as the emitter and receiver, respectively. The inset shows a magnified image of one of these disks. (c) Scattering image of a plasmonic ellipse. The Ag disk at the left focal point is excited with a focused HeNe laser with radial polarization; the direct reflection of the laser from the focal point is blocked with a circular spatial filter.

fluorophore *via* SPPs.[20] Moreover, plasmonic waveguides[21−23] can be used to direct SPPs launched by an emitter to a receiver along a one-dimensional structure, providing a direct connection for energy transfer.[24−28] However, whereas such plasmonic waveguides can, in principle, lead to highly directional energy flow, they also have several disadvantages. For example, they exhibit significant sensitivity to defects because only a single channel connects the donor to the acceptor, and enhanced field confinement leads to a trade-off between high coupling efficiency and long propagation distance.[29]

Here, we explore plasmonic resonators with an elliptical shape as a possible structure to overcome these limitations. Due to their geometry, elliptical resonators can enable defect-tolerant plasmon-mediated energy transfer over long distances. Indeed, the utility of the ellipse for photonics has long been recognized. In 1931, Synge proposed an optical microscope with a hollow (three-dimensional) ellipsoid with reflective walls.[30] If a source is placed at one focal point of the ellipse, all emitted light would be directed to the other focal point upon reflection from the walls. We exploit a two-dimensional (2D) plasmonic analogue, in which a region of flat Ag surface is surrounded by an elliptical block reflector (Figure 1). This structure, which can be fabricated using standard lithographic techniques, collects all SPPs emitted at one focal point and directs them to the other focal point, independent of the emission direction of the initial SPP. Consequently, the plasmonic ellipse is highly tolerant to local defects because energy is transferred through many paths simultaneously.

Flat elliptical resonator structures have previously been realized, and it was shown that they mimic quantum corrals[31] or serve as unidirectional, broad-band scatterers.[32] Transferring energy at a single frequency from one focal point to the other was first investigated by Drezet *et al.*[33] using an elliptically shaped Bragg reflector on a gold surface. More recently, elliptical cavities have been milled into single-crystalline Au flakes to coherently couple two whispering-gallery-mode antennas separated by distances up to 2 μm.[34,35]

We present a plasmonic elliptical resonator where SPPs mediate energy transfer over 10 μm between ensembles of quantum emitters. To first characterize our resonator, we place scattering Ag disks as plasmon sources at the focal points of the ellipse. Locally excited plasmons then propagate along closed paths inside the ellipse, leading to resonator modes. We investigate these modes by measuring broad-band transmission spectra between the focal points and discuss their influence on energy transfer. Crucial for practical realizations, the defect tolerance of the plasmonic ellipse is assessed by measuring the transmitted signal in the presence of micrometer-sized obstructions placed between the foci. Finally, to demonstrate energy transfer between quantum emitters, we print colloidal quantum dots (QDs) at the focal points of the plasmonic ellipse. We study the dynamics of energy transfer between the QDs with time- and spectrally resolved measurements and show that these dynamics can be captured well using a rate-equation model. Hence, our findings demonstrate that plasmonic ellipses can provide defect-tolerant energy transfer across long distances.

RESULTS AND DISCUSSION

The schematic in Figure 1a highlights the two key properties of plasmonic ellipses for energy transfer. First, every SPP ray leaving one focal point (F_1) will arrive at the other focal point (F_2) after a single reflection at the resonator wall. Second, the path length with one reflection between the two focal points is always equal to twice the long half-axis of the ellipse, 2*a*. This property ensures that all SPPs launched at F_1 interfere constructively at F_2, independent of the emission direction of the initial ray and the direct distance between the focal points, 2*e*.

We fabricate our plasmonic elliptical resonator structures using template stripping.[36,37] First, an elliptical groove is patterned into a Si substrate using electron-beam lithography followed by HBr plasma etching. Then, Ag is evaporated onto the patterned Si chip and removed *via* template stripping (see Methods and section S1 in the Supporting Information for details). The result is a smooth silver surface with roughness down to 0.3 nm root-mean-squared[37] that is surrounded by an elliptical Ag protrusion acting as a reflector for SPPs. The scanning electron micrograph (SEM) in Figure 1b shows such a resonator with a protrusion that is ∼600 nm high and 2 μm wide. The focal points of the ellipse are separated by 2*e* = 10 μm and the long half-axis of the ellipse is *a* = 8 μm. These parameters, which provide a good compromise between large focal-point separation and sufficient energy transfer, are used throughout this work.

In our optical experiments, we use two methods to excite SPPs at the focal points. The first approach is to focus laser

DOI: 10.1021/acsnano.9b03201
ACS Nano 2019, 13, 9048−9056

light at a Ag disk precisely placed at the focal point (see inset in Figure 1b). These disks (200 nm in diameter and 100 nm in height) can be incorporated into the fabrication process using electron-beam lithography. They allow for broad-band coupling of free-space light into SPPs in the ellipse (see section S2 and Figure S1 in the Supporting Information for details). Specifically, we utilize a radially polarized laser beam to create a strong longitudinal electric-field component in the center of the focus.[1,38] This electric-field component excites a dipole moment in the Ag disk normal to the flat metal surface, which then couples efficiently to transverse-magnetic SPP modes.[17] In contrast to plasmon excitation by scattering of a linearly polarized laser beam,[33] the symmetry of the radially polarized laser beam ensures that SPPs are launched isotropically in-plane. The second approach to launch SPPs in the ellipse relies on near-field coupling to fluorescent QDs,[39] placed precisely in the focal points using electrohydrodynamic nanodripping (see Methods and section S1 in the Supporting Information).[22,40] After exciting the QDs locally with a focused laser, they launch SPPs into the ellipse.

Figure 1c shows an image formed on an electron-multiplying charge-coupled device (EMCCD) camera of an ellipse for which a radially polarized HeNe laser (λ = 632.8 nm) was focused onto the Ag disk placed at F_1. The image shows a bright spot at F_2, where the second Ag disk scatters the SPPs that arrive at the receiver into photons—evidence that the plasmonic ellipse can mediate energy transfer. The direct reflection of the excitation laser from F_1 is blocked using a spatial filter in an intermediate image plane in the optical path (see Methods and Figure S2 in the Supporting Information). The halo around F_1 is caused by the excitation laser that is not blocked by the circular spatial filter.

Additionally, we observe a particular intensity pattern along the reflector wall. To explain this, we must consider that a portion of the SPPs leaving F_1 do not scatter at F_2 but propagate back toward F_1. Hence, to first order, any particular point along the reflector wall can be reached by SPPs coming from F_1 *via* two separate paths: either directly or after one reflection and passage through F_2. The difference in the path length leads to either constructive or destructive interference of SPPs at any point along the reflector (see section S3 and Figure S3 in the Supporting Information for further details). The particular spatial interference pattern at the frequency of the HeNe laser is visible along the reflector wall in Figure 1c.

To this point, we have explained the plasmonic ellipse using a ray picture (*i.e.*, rays of SPPs propagating from F_1 to F_2). However, if the phase that an SPP accumulates during one round trip from F_1 to F_2 and back to F_1 is a multiple of 2π, a source of SPPs at F_1 self-interferes constructively, leading to a resonance.[32] Importantly, this round-trip phase depends on the round-trip length $4a$, the SPP wavelength, and the phase difference imparted by the two reflections, but not on the distance between the focal points $2e$. The occurrence of resonances leads to a second equivalent picture where the plasmonic ellipse is treated as a resonator with particular eigenmodes (*i.e.*, standing waves) that can be excited.

To achieve energy transfer between quantum emitters, which have characteristic absorption and emission spectra, energy is transferred by coupling the emitter and receiver to the same eigenmode of the elliptical resonator. Every eigenmode is characterized by a resonance frequency and its spatial electric-field-intensity distribution. For energy transfer, both the spectral and spatial overlap of the donor and acceptor with the eigenmodes are essential.

To probe the eigenmode spectrum supported by our particular resonator, we utilized broad-band light generated from a sapphire crystal and a 1040 nm pulsed laser (see Methods). The resulting supercontinuum pulses were focused onto the Ag disk at F_1, launching broad-band SPPs into the resonator. Spectra were then collected for those SPPs that were scattered at the second Ag disk at F_2 using an imaging spectrograph. Figure 2a shows the transmission spectrum from F_1 to F_2 for our plasmonic ellipse. This spectrum reveals all resonator modes that lie within the supercontinuum bandwidth (~550 to 650 nm, black dotted line in Figure 2a)

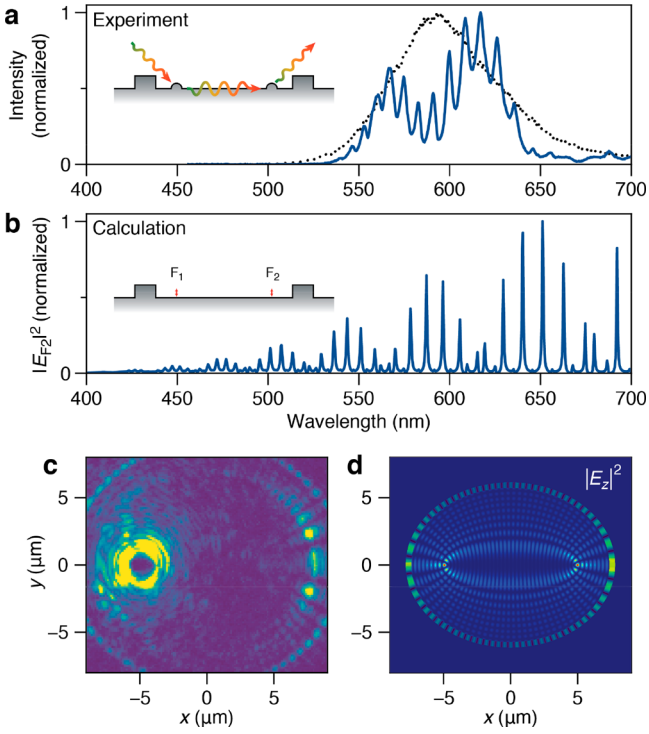

Figure 2. Transmission spectrum and eigenmode analysis of the plasmonic elliptical resonator. (a) Experimental transmission spectrum (blue line) from F_1 to F_2 of an ellipse with distance $2e$ = 10 μm between the focal points and long half-axis a = 8 μm. The spectrum is measured by focusing a broad-band supercontinuum laser beam on a Ag disk at F_1 and collecting the scattered photons from SPPs arriving at a Ag disk at F_2. The black dotted line shows the reflection spectrum of the excitation laser focused on a flat Ag surface for comparison (see also Figure S4 in the Supporting Information). (b) Frequency-domain simulation with COMSOL Multiphysics of the transmission spectrum of an ellipse with the same parameters as in (a). An electric point-dipole source was placed at F_1, and the electric-field intensity at F_2 was measured as a function of wavelength. (c) Image of an elliptical resonator (without Ag disk at F_2), excited with a radially polarized HeNe laser source (λ = 632.8 nm) focused at F_1. Along the reflector, SPPs are scattered with an intensity modulation characteristic for the excited eigenmode. (d) Electric-field intensity distribution of the ellipse eigenmode closest to the HeNe wavelength, calculated using COMSOL Multiphysics. The electric-field intensity shows two strong maxima at the focal points of the ellipse, indicating that this mode is useful for energy transfer. At the position of the inner reflector wall, the electric-field intensity of the eigenmode is plotted to allow direct comparison with the scattered SPP intensity in the experiment (panel c).

DOI: 10.1021/acsnano.9b03201
ACS Nano 2019, 13, 9048−9056

and are excited by the first Ag disk. In contrast to smaller plasmonic ellipses ($a \sim 1$ μm),[31,32] our structure has many eigenmodes. However, only the modes where the electric-field intensity is strongly concentrated at the two focal points of the ellipse are detected in the transmission spectrum and contribute to the energy transfer. This explains the different peak amplitudes of the eigenmodes in Figure 2a, which are determined by the electric-field intensities at the two focal points. The observed eigenmodes are spectrally separated by ~6.7 nm and have a full width at half-maximum line width of ~5 nm at 550 nm. Based on these numbers, we can estimate a quality factor of $Q \approx 110$ and a finesse of $\mathcal{F} \approx 1.3$ for this particular resonator. Compared to Ag nanowires, previously used for plasmon-mediated energy transfer, our Q is higher by a factor of 2.[41] The resonator finesse and the emission and absorption spectra of the quantum emitters determine whether one or several of the resonator eigenmodes contribute to the energy-transfer process.

The eigenmodes that we detect in the transmission spectrum for our plasmonic ellipse can be understood by performing frequency-domain finite-element calculations with COMSOL Multiphysics (see section S3 in the Supporting Information). It has already been shown[32] that a simple dispersive plasmonic Fabry–Pérot resonator model can predict the approximate wavelength spacing of the resonance peaks of an elliptical structure (see section S3 and Figure S4 in the Supporting Information) but not the relative coupling strength of the source and receiver to these modes.[2] Our model can calculate both. We consider an electric dipole source perpendicular to the surface placed at focal point F_1 and evaluate the electric-field intensity polarized normal to the surface at focal point F_2. Figure 2b shows the calculated transmission spectrum for an ellipse with the same dimensions as in the experiments (but without Ag disks at the focal points). It shows multiple sets of resonances, each with an intensity modulated due to the wavelength-dependent electric-field overlap between the eigenmode and the dipole (see section S3 in the Supporting Information). The individual resonances have line widths down to 1 nm and peak spacings of 6.5 nm (at 550 nm). From these values, we obtain a resonator quality factor of $Q \approx 550$ and a finesse of $\mathcal{F} \approx 6.5$, numbers that are significantly higher than the values determined from experiment. Most likely, this discrepancy results from higher losses in our experimental structure such as out-scattering at the Ag disks, increased ohmic losses in the metal, and lower reflectance at the reflector. Nevertheless, our simulation qualitatively captures the experimental transmission spectrum shown in Figure 2a and its particular intensity modulations. The finite size of the Ag disks in contrast to the point dipole used in the model can explain the deviation in the resonance position between the simulated and experimental transmission spectrum (see section S3 and Figure S4 in the Supporting Information). From the transmission spectrum, we conclude that the plasmonic ellipse supports many resonant modes with closely spaced frequencies that couple focal points F_1 and F_2 with a strength depending on their spatial electric-field distributions.

The spatial electric-field intensity distribution of a single eigenmode can also be probed experimentally. For example, by exciting a Ag disk at F_1 of the elliptical resonator with the single-frequency HeNe laser, SPP out-scattering along the edge of the ellipse can be observed (Figure 2c). It is known that when SPPs hit a block reflector, a small fraction of their intensity is scattered into photons.[42] In our experiment, this appears as out-scattering with an intensity proportional to the SPP electric-field intensity at the reflector. The intensity profile observed along the elliptical reflector in Figure 2c is characteristic for the excited eigenmode. Qualitatively, this modulation can be understood in terms of two SPP rays that interfere at the reflector because they arrive through different paths from F_1 (see section S3 and Figure S3 in the Supporting Information). Figure 2d shows the full intensity distribution of the electric-field component perpendicular to the Ag surface of the eigenmode ($\lambda = 632.6$ nm) closest to the HeNe wavelength calculated with COMSOL Multiphysics. In addition to an intensity profile along the edge of the ellipse that is similar to what we observe experimentally (Figure 2c), the calculated eigenmode shows two strong intensity maxima at the foci of the ellipse where the emitter and receiver are placed. This strong confinement of the electric field is beneficial for the energy-transfer efficiency of plasmonic ellipses compared to a flat Ag interface. However, because

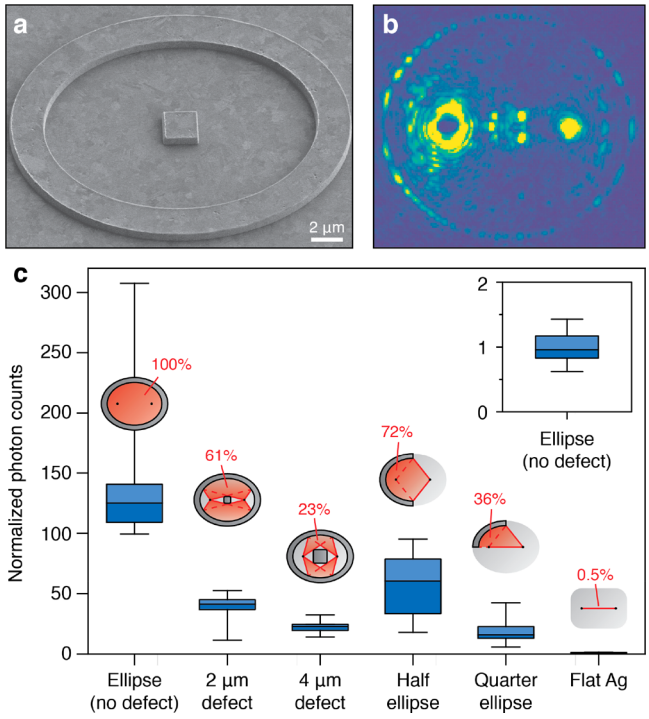

Figure 3. Defect tolerance of plasmonic ellipses. (a) SEM of a template-stripped elliptical resonator ($2e = 10$ μm, $a = 8$ μm) with a square defect of $d = 2$ μm side length. (b) Scattering image of a plasmonic ellipse containing a defect ($d = 2$ μm). A radially polarized HeNe laser ($\lambda = 632.8$ nm) is used to excite the ellipse at the left focal point. (c) Boxplot (horizontal line inside box indicates median value; the box extends from the lower to upper quartile values of the data; whiskers highlight span of data points) comparing the intensity of scattered SPPs at the acceptor for six ellipses without a defect, nine ellipses with a $d = 2$ μm defect, five ellipses with a $d = 4$ μm defect, nine half ellipses, nine quarter ellipses, and nine structures without an elliptical reflector. For each case, nine nominally identical ellipses were fabricated. Structures in which one of the Ag disks were missing were rejected based on dark-field microscopy images (see Figure S5 in the Supporting Information). The mean scattered SPP intensity measured for two Ag disks without an elliptical resonator (inset) was used to normalize the data. Schematic insets provide an estimate of the percentage of SPPs arriving at the acceptor position compared to a plasmonic ellipse without defect.

DOI: 10.1021/acsnano.9b03201
ACS Nano 2019, 13, 9048–9056

the electric-field hot spots at the focal points are as tight as ~200 nm in the lateral direction, precise placement of the donor and acceptor at the foci is required.

Reliable transfer of energy from emitter to receiver also requires tolerance to defects. Energy transfer in Ag nanowires or on flat Ag surfaces would be completely inhibited when a fabrication imperfection (*e.g.*, dust particle) disrupts the direct path between donor and acceptor. This problem can, in principle, be alleviated in ellipses, where energy is transferred from F_1 to F_2 along many different paths. Figure 3a shows an electron micrograph of a plasmonic ellipse containing an intentionally placed square defect with a side length of d = 2 μm and the same height as the reflector (600 nm). We measure the plasmons transmitted between the two focal points by focusing a radially polarized HeNe laser beam onto the Ag disk placed at F_1 (left scatterer in Figure 3a) and imaging the signal scattered by the ellipse on an EMCCD camera (Figure 3b). Despite the large defect, the bright spot at F_2 indicates that an appreciable amount of plasmons arrived at the acceptor. The SPPs scattered from the edges of the defect also indicate that energy is lost.

We quantify the relative amounts of energy lost because of the defect by comparing defect-free ellipses to those containing two different sizes of defects (d = 2 and 4 μm). Minor differences in fabrication are averaged out by measuring the signal from 5–9 nominally identical resonators for each group on the same sample (see Figure S5 in the Supporting Information for dark-field images of all resonators). For each measurement, we excited F_1 with a radially polarized HeNe laser and integrated the signal scattered at F_2 over an area of 1.3 × 1.3 μm^2. Figure 3c shows a boxplot of the measured intensity normalized to the mean intensity of two Ag disks that are separated by the same distance (10 μm) but placed on a flat Ag film without any reflectors. The presence of the elliptical resonator enhances the transferred signal by a factor of ~125 (median value). Placing a 2 μm defect between the donor and acceptor reduces the signal by a factor of only 3 compared to an ellipse without a defect. A 4 μm defect reduces the signal by a factor of 5.5, but the structure still transmits 24 times more SPPs than a flat Ag surface absent of any structuring. Removing one-half or three-quarters of the ellipse reduces the transmitted signal by a factor of 2 and 7.9, respectively. With a very simple model (red-shaded segments and corresponding percentage values in Figure 3c), we calculated the fraction of emission angles from F_1 for which an SPP ray ends up at F_2 after one reflection. This model qualitatively reproduces the reduction of plasmon transmission that we measured upon introduction of an intentional defect.

So far, we have characterized the properties of our plasmonic ellipses by directly exciting the resonator modes with a laser source. To show energy transfer between quantum emitters, we also performed experiments with colloidal QDs. Due to their size-tunable optical properties, QDs can be synthesized to emit and absorb light across the visible spectrum.[43] Figure 4a shows the absorption (dotted lines) and emission (solid lines) spectra of the two types of CdSe-based core/shell QDs used in this work (see Methods and section S1 in the Supporting Information for details). Photoexcited QDs show fluorescence from clearly defined band-edge electronic states but, in contrast to fluorescent molecules, can absorb all photons of higher energy. This property facilitates the energy transfer from donor to acceptor QDs as the emission from QDs emitting at higher energy (here, green) always overlaps with the absorption of QDs emitting at lower energy (here, red). The green-emitting QDs (green lines in Figure 4a) can thus act as donors and red-emitting QDs (red lines) as acceptors.

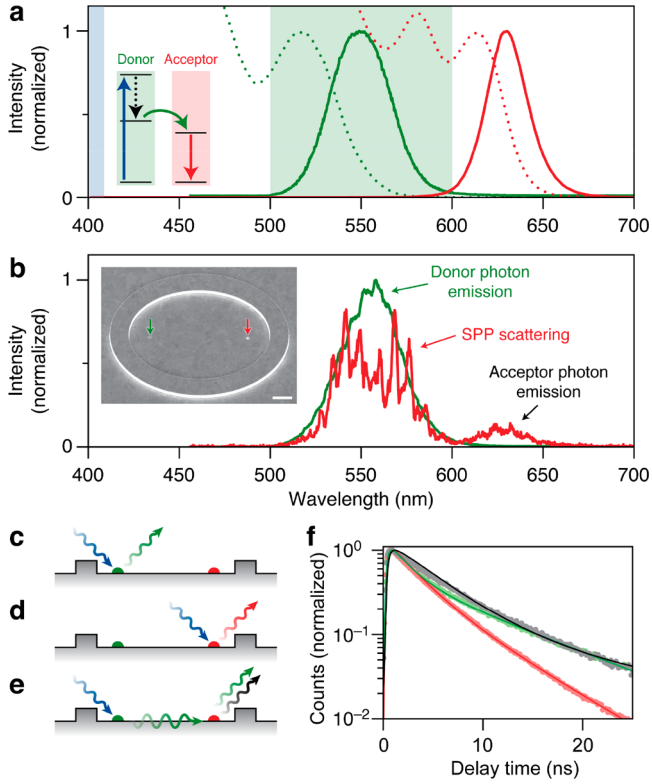

Figure 4. Energy transfer between colloidal CdSe-based core/shell QDs in a plasmonic ellipse. (a) Emission (solid lines) and absorption (dotted lines) spectra for the two types of QDs used. Both were dispersed in hexane (see Methods for QD sizes). The spectrum of the green donor QDs overlaps with the absorption spectrum of the red acceptor QDs. The inset schematically shows the energy-transfer process involving the 405 nm laser pump (blue arrow), the cooling to the band-edge of the donor (black dotted arrow), the energy transfer mediated by SPPs (green arrow), and the acceptor fluorescence (red arrow). (b) Photon signals measured at the donor (green line) and acceptor (red line) when the donor QD is excited with a focused laser spot. The inset shows an SEM of the plasmonic ellipse with small ensembles (~1000) of donor and acceptor QDs at the two focal points (2 μm scale bar). (c–e) Excitation and detection schemes for the time-resolved measurements. (f) Time-resolved measurements for the three situations presented in (c–e). The green and red data correspond to the independent excitation and detection of the donor and acceptor QDs, as depicted in (c) and (d), respectively. The gray data correspond to the situation in (e), where a 590 nm long-pass filter is used to isolate the acceptor photon emission from the SPP scattering contribution. A rate-equation model (solid lines; see section S3 in the Supporting Information for details) captures the dynamics of the decay traces, confirming energy transfer in our plasmonic ellipses.

To demonstrate plasmon-mediated energy transfer in our elliptical resonator, we printed subwavelength-sized ensembles of QDs (~1000 QDs) at the two focal points (inset of Figure 4b). The green line in Figure 4b shows the signal measured from the location of the green QDs (inset Figure 4b, green arrow) when they are directly excited with a 405 nm pulsed laser source. This spectrum contains a single broad peak at ~550 nm, which is at the same position as the green fluorescence in Figure 4a. After photoexcitation, the excitons

DOI: 10.1021/acsnano.9b03201
ACS Nano 2019, 13, 9048–9056

created in the green QDs quickly relax to the band edge (~picosecond time scale).[44] Therefore, we attribute this spectrum to band-edge fluorescence of the green donor QDs. The weak fluorescence intensity modulation at the frequencies of the resonator modes can be attributed to competition between SPP excitation and photon emission.

The red line in Figure 4b corresponds to the photon signal measured at the location of the red acceptor QDs at F_2 (inset Figure 4b, red arrow), upon laser excitation of the green donor QDs at F_1. This signal contains two main features. The first feature at ~550 nm spectrally overlaps with the donor emission and can, therefore, be attributed to SPPs launched by the donor that are scattered into green photons at the acceptor. The closely spaced peaks in this scattering signal show that the donor is coupled to the resonances of the ellipse. The second feature at ~630 nm overlaps with the acceptor emission spectrum (cf. Figure 4a). This signal suggests plasmon-mediated energy transfer: acceptor fluorescence after photoexcitation of the donor. Importantly, energy transfer occurs here over QD−QD separations as large as 10 μm—a distance that is 3 orders of magnitude larger than typical distances for Förster energy transfer (<10 nm) through near-field coupling[45−47] and 15% larger than previously achieved for SPP-mediated single-channel energy transfer on Ag nanowires.[28] This distance can be extended even further (see Figure S6 in the Supporting Information for energy-transfer measurements in elliptical resonators with $2e$ = 15 μm), but maximization of the emitter−acceptor separation was not the goal of this work.

For a more complete analysis, we also performed time-resolved measurements on the donor and acceptor QDs. Figure 4f shows the photoluminescence decay traces for the three different configurations shown in Figure 4c−e. The green and red traces correspond to the situations in Figure 4c,d, where the donor and acceptor QDs are excited and detected independently. In this way, the dynamics of the donors and acceptors are determined separately. The gray trace corresponds to the situation in Figure 4e, where the donor is excited with the laser pulse, and the signal from the acceptor is detected. In this case, a 590 nm long-pass filter was placed before the detector to filter out the scattering of green SPPs, emitted by the donor, from the acceptor signal.

The separate dynamics of the donor QDs (green data in Figure 4f) and acceptor QDs (red data) both show multiexponential decay, presumably due to variations in the QDs or in the QD-to-SPP coupling.[48] Compared to the decay of the donor QDs in a tetradecane dispersion, the decay of the donor QDs that are printed in the focus of the ellipse is shorter because of QD-to-SPP coupling and self-quenching of the QDs in the assembly (see Figure S7 in the Supporting Information). The evidence for energy transfer lies in the photoluminescence decay of the acceptor after photoexcitation of the donor (gray data). The acceptor emission decays more slowly when excited indirectly *via* the donor QDs (gray data) than when excited directly (red data). Due to the long exciton lifetime of the green QDs, they feed the red QDs over tens of nanoseconds. Therefore, the slow decay of the green QDs influences the signal from the red QDs. We would also have expected a rise of a few nanoseconds in the emission signal from the acceptor QDs upon excitation of the donor QDs. However, this effect is hardly observable in our experimental data (see Figure S8 in the Supporting Information). The rise of the red emission may be hidden in our experiments because, in addition to energy transfer from the donor QDs, the red emission may be directly excited by our 405 nm laser beam. This can occur if the focused laser spot is scattered by the QDs at F_1, thus generating 405 nm SPPs that travel outward and are focused to F_2 by the resonator structure.

To quantify the contributions to the red emission from the donor-to-acceptor energy transfer and the direct excitation by 405 nm SPPs, we developed an analytical model (see section S4 and Figure S9 in the Supporting Information) that describes the expected photoluminescence decay dynamics including both contributions. The solid lines in Figure 4f show the result of fitting the data to this model. From the fit, we conclude that approximately 34% of the acceptor signal originates from donor-to-acceptor energy transfer, and 66% of the signal is due to direct excitation of the acceptor by 405 nm SPPs. In Figure S6 in the Supporting Information, we show results from reference measurements for which the green donor QDs were photobleached. These confirm that the red acceptor QDs at F_2 are in part excited by 405 nm SPPs in-scattered at F_1. Our resonator structure thus facilitates donor-to-acceptor transfer between quantum emitters over a distance as large as 10 μm, even by 405 nm SPPs scattered in at the donor location, despite the low propagation length of SPPs at the excitation laser wavelength (L_{SPP} = 5.5 μm at λ = 405 nm).

We also estimate the overall donor-to-acceptor energy-transfer efficiency in our structures. Based on values reported in the literature, we assume that the exciton-to-SPP coupling efficiency is ~40%.[27,49] Whereas the SPP-to-exciton coupling is very challenging to quantify, we optimistically assume this efficiency to also be ~40% in our case. The SPP reflectivity r of our block reflectors was measured above 0.9,[23,42] and the SPP propagation length L_{SPP} is 40 μm at λ = 550 nm.[37] Using these values, we obtain an overall transfer efficiency of $0.4 \times 0.4 \times r \times e^{-2a/L_{SPP}} \cong 10\%$ for QD-to-QD transfer. This value is orders of magnitude higher than photon-mediated energy transfer in free space for the same donor−acceptor separation.[1]

CONCLUSIONS

We have shown that plasmonic elliptical resonators support eigenmodes with strong electric-field maxima at the two focal points. These eigenmodes with quality factors up to Q = 110 can be excited by a scattering Ag disk or quantum emitters that are placed at one of the focal points. By printing donor and acceptor QDs with overlapping emission and absorption spectra at each focal point respectively, energy can be transferred *via* SPPs across 10 μm—a distance that is 15% longer than reported for Ag nanowires.[28] Compared to flat Ag, the elliptical resonator enhances energy transfer by a factor of 125 for a donor−acceptor separation of 10 μm. Further, we set up a rate-equation model that captures the most important dynamics of donor excitation, energy transfer, and acceptor recombination. Due to the full collection angle of the ellipse, energy transfer within our resonators is tolerant to 4 μm defects that block the direct path between donor and acceptor. Thus, despite their larger footprint, elliptical resonators offer a valuable alternative to Ag nanowires for plasmon-mediated energy transfer because of their defect tolerance and enhanced energy-transfer distance. Further, our findings highlight the potential of elliptical resonators as a platform for long-range energy transfer and allow investigations of the coupling of single quantum emitters placed in such structures.

DOI: 10.1021/acsnano.9b03201
ACS Nano 2019, 13, 9048−9056

METHODS

Fabrication of Plasmonic Elliptical Resonators. Plasmonic elliptical resonator structures were fabricated using template stripping.[36] Templates for elliptical resonators containing scattering Ag disks were prepared by a two-step electron-beam (e-beam) process. Disks with 200 nm diameter, which defined the scatterers, were created using e-beam lithography (Vistec, NFL 5). After developing the sample, approximately 100 nm deep holes were etched into the Si chips using HBr-based inductively coupled plasma etch (Oxford Instruments, PlasmaPro 100 Cobra, 80 W) for 35 s. Finally, the resist was removed. The elliptically shaped block reflectors were fabricated in a second step where elliptical annuli with 2 μm width were defined with e-beam lithography. Before removing the resist, approximately 600 nm deep trenches were etched into the Si chips using the same HBr-based inductive coupled plasma etch for 2.5 min. For samples without Ag disks, only the second lithography step was applied.

A thermal evaporator (Kurt J. Lesker, Nano36) was used to deposit Ag films. Deposition of a 1 μm thick Ag film onto the ellipse templates was performed at high rates (>25 Å s^{-1}) and low residual gas pressures (3×10^{-7} mbar).[37] The deposited Ag film was template-stripped by bonding a microscope slide to the film using an ultraviolet-light-curable epoxy (EpoTek, OG142-95). The Ag-epoxy-glass stack was then stripped from the template to reveal elliptical resonators. More detail on the sample fabrication is available in section S1 of the Supporting Information.

Electrohydrodynamic Nanodripping of QDs. For electrohydrodynamic nanodripping, we used two inks based on green and red QDs. Dispersions in hexane of green CdSe/ZnS core/shell QDs with a compositionally graded shell (~10 nm particle diameter, emission at ~550 nm, synthesized according to a protocol described by Prins *et al.*[50]) and red CdSe/CdS/ZnS core/shell QDs (~4.1 nm core diameter, emission at ~630 nm, synthesized according to a protocol described by Kress *et al.*[23]) were prepared. Hexane was then replaced by tetradecane as the solvent of the QD dispersions and the concentration of the green and red ink was adjusted to an optical density of 2 and 0.5, respectively (measured at the lowest energy exciton peak in a spectrometer, using a quartz cuvette with a 1 mm path length). For electrohydrodynamic nanodripping of QDs, a direct current electric potential of ~220 V was applied between a metal-coated nozzle (+) and the template-stripped silver substrate (ground) to eject ink. Each ensemble of QDs was printed at a separation of around 5 μm between the nozzle and the plasmonic substrate by applying a voltage pulse for 120 ms. A complete description of the preparation of QD inks and printing setup is available in section S1 of the Supporting Information.

Optical Measurements. Our experimental setup, which allows multiple excitation and detection schemes, is shown in Figure S2 of the Supporting Information. The sample is mounted on an inverted microscope (Nikon, Eclipse Ti−U) equipped with a 100× air objective (Nikon, TU Plan Fluor; numerical aperture of 0.9). To directly launch SPPs by scattering off a Ag disk, we used a single-mode fiber-coupled HeNe laser (Thorlabs HNL100R, 632.8 nm wavelength) or a supercontinuum generated from a sapphire crystal using a 1040 nm pump laser (Spectra-Physics, Spirit 1040-8). A broad-band polarizing beam splitter cube (Thorlabs, CCM1-PBS251) in combination with a Q-plate (ArcOptix, S-PLATE) converts linear polarization into radial polarization. To filter out higher-order transverse modes, the beam is focused through a 15 μm pinhole using two lenses. A multiwave liquid-crystal variable retarder (Thorlabs, LCC2415) is used to correct for birefringence of the optical components in the setup. The radially polarized laser beam was directed to the sample using a broad-band 50/50 beam splitter (AHF analysentechnik) and focused with the microscope objective. To excite QDs, a 405 nm laser diode (Picoquant, D-C-405) was directed to the sample using a dichroic beam splitter (488 nm long pass, AHF analysentechnik).

Emission from the sample was collected by the objective and sent through the beam splitter and relay lenses (focal length of 200 mm) into an imaging spectrometer (Andor, Shamrock 303i). A circular spatial filter (Cr evaporated on a coated glass window from Thorlabs, WG11010-A), placed in an intermediate image plane, was used to block the strong reflection of the laser spot. The emission was dispersed with a grating of 150 lines/mm (500 nm blaze) and imaged with an air-cooled electron-multiplying charged-coupled device camera (Andor, iXon 888 Ultra). Real-space images were obtained using the zero-order mode of the same grating. For fluorescence measurements, an emission filter (500 nm long-pass, AHF analysentechnik) was placed directly after the dichroic beam splitter to filter out the 405 nm excitation light. For time-resolved measurements, the emission was focused onto an avalanche photodiode (Excelitas, SPCM-AQRH-14-TR) connected to a time-tagger box (Picoquant, PicoHarp 300).

ASSOCIATED CONTENT

Supporting Information

The Supporting Information is available free of charge on the ACS Publications website at DOI: 10.1021/acsnano.9b03201.

Detailed description of our sample fabrication, optical setup, and numerical models (sections S1−S4); parameters used in our rate-equation model (Tables S1−S4); additional data supporting our analysis (Figures S1−S9) (PDF)

AUTHOR INFORMATION

Corresponding Author

*E-mail: dnorris@ethz.ch.

ORCID

Felipe V. Antolinez: 0000-0002-1787-0112
Jan M. Winkler: 0000-0001-5062-8523
Patrik Rohner: 0000-0002-5524-0402
Stephan J. P. Kress: 0000-0001-7034-9310
Robert C. Keitel: 0000-0002-9412-8034
Jian Cui: 0000-0002-2394-3357
Freddy T. Rabouw: 0000-0002-4775-0859
Dimos Poulikakos: 0000-0001-5733-6478
David J. Norris: 0000-0002-3765-0678

Present Addresses

[§]Helmholtz Zentrum München, Ingolstadter Landstrasse 1, 85764 Neuherberg, Germany.
[⊥]Debye Institute for Nanomaterials Science, Utrecht University, Princetonplein 1, 3584 CC Utrecht, The Netherlands.

Author Contributions

F.V.A. and J.M.W. contributed equally and are listed alphabetically.

Notes

The authors declare no competing financial interest.

ACKNOWLEDGMENTS

This work was supported by the European Research Council under the European Union's Seventh Framework Program (FP/2007-2013)/ERC Grant Agreement No. 339905 (QuaDoPS Advanced Grant) and the Swiss National Science Foundation under Award No. 200021-165559. F.T.R. acknowledges support from The Netherlands Organization for Scientific Research (NWO, Rubicon Grant 680-50-1509). We thank B. le Feber, R. Brechbühler, L. Novotny, and L. Martín-Moreno for stimulating discussions, and U. Drechsler, S. Meyer, A. Olziersky, and H. Rojo for technical assistance.

DOI: 10.1021/acsnano.9b03201
ACS Nano 2019, 13, 9048−9056

REFERENCES

(1) Novotny, L.; Hecht, B. *Principles of Nano-Optics*; Cambridge University Press: Cambridge, UK, 2012; pp 257−264.
(2) Martín-Cano, D.; Martín-Moreno, L.; García-Vidal, F. J.; Moreno, E. Resonance Energy Transfer and Superradiance Mediated by Plasmonic Nanowaveguides. *Nano Lett.* **2010**, *10*, 3129−3134.
(3) Förster, T. Zwischenmolekulare Energiewanderung Und Fluoreszenz. *Ann. Phys.* **1948**, *437*, 55−75.
(4) Imamoglu, A.; Awschalom, D. D.; Burkard, G.; DiVincenzo, D. P.; Loss, D.; Sherwin, M.; Small, A. Quantum Information Processing Using Quantum Dot Spins and Cavity QED. *Phys. Rev. Lett.* **1999**, *83*, 4204−4207.
(5) Evans, R. E.; Bhaskar, M. K.; Sukachev, D. D.; Nguyen, C. T.; Sipahigil, A.; Burek, M. J.; Machielse, B.; Zhang, G. H.; Zibrov, A. S.; Bielejec, E.; Park, H.; Lončar, M.; Lukin, M. D. Photon-Mediated Interactions between Quantum Emitters in a Diamond Nanocavity. *Science* **2018**, *362*, 662−665.
(6) Childress, L.; Taylor, J. M.; Sørensen, A. S.; Lukin, M. D. Fault-Tolerant Quantum Communication Based on Solid-State Photon Emitters. *Phys. Rev. Lett.* **2006**, *96*, No. 070504.
(7) Koenderink, A. F.; Alu, A.; Polman, A. Nanophotonics: Shrinking Light-Based Technology. *Science* **2015**, *348*, 516−520.
(8) Lodahl, P.; Mahmoodian, S.; Stobbe, S. Interfacing Single Photons and Single Quantum Dots with Photonic Nanostructures. *Rev. Mod. Phys.* **2015**, *87*, 347−400.
(9) Chang, D. E.; Douglas, J. S.; González-Tudela, A.; Hung, C. L.; Kimble, H. J. Colloquium: Quantum Matter Built from Nanoscopic Lattices of Atoms and Photons. *Rev. Mod. Phys.* **2018**, *90*, 31002.
(10) Andrew, P.; Barnes, W. L. Forster Energy Transfer in an Optical Microcavity. *Science* **2000**, *290*, 785−788.
(11) Zhong, X.; Chervy, T.; Zhang, L.; Thomas, A.; George, J.; Genet, C.; Hutchison, J. A.; Ebbesen, T. W. Energy Transfer between Spatially Separated Entangled Molecules. *Angew. Chem., Int. Ed.* **2017**, *56*, 9034−9038.
(12) Deshmukh, R.; Biehs, S. A.; Khwaja, E.; Galfsky, T.; Agarwal, G. S.; Menon, V. M. Long-Range Resonant Energy Transfer Using Optical Topological Transitions in Metamaterials. *ACS Photonics* **2018**, *5*, 2737−2741.
(13) Saleh, B. E. A.; Teich, M. C. *Fundamentals of Photonics*; Wiley: New York, 1991; pp 289−324.
(14) Abbe, E. Beiträge Zur Theorie Des Mikroskops Und Der Mikroskopischen Wahrnehmung: I. Die Construction von Mikroskopen Auf Grund Der Theorie. *Arch. für mikroskopische Anat.* **1873**, *9*, 413−418.
(15) Andrew, P.; Barnes, W. L. Energy Transfer across a Metal Film Mediated by Surface Plasmon Polaritons. *Science* **2004**, *306*, 1002−1005.
(16) Reil, F.; Hohenester, U.; Krenn, J. R.; Leitner, A. Förster-Type Resonant Energy Transfer Influenced by Metal Nanoparticles. *Nano Lett.* **2008**, *8*, 4128−4133.
(17) Maier, S. A. Plasmonics: Fundamentals and Applications. *Plasmonics: Fundamentals and Applications*; Springer: New York, 2007; pp 21−52.
(18) Anger, P.; Bharadwaj, P.; Novotny, L. Enhancement and Quenching of Single-Molecule Fluorescence. *Phys. Rev. Lett.* **2006**, *96*, 113002.
(19) Chang, D. E.; Sørensen, A. S.; Hemmer, P. R.; Lukin, M. D. Quantum Optics with Surface Plasmons. *Phys. Rev. Lett.* **2006**, *97*, No. 053002.
(20) Bouchet, D.; Cao, D.; Carminati, R.; De Wilde, Y.; Krachmalnicoff, V. Long-Range Plasmon-Assisted Energy Transfer between Fluorescent Emitters. *Phys. Rev. Lett.* **2016**, *116*, 037401.
(21) Bozhevolnyi, S. I.; Volkov, V. S.; Devaux, E.; Laluet, J.-Y. Y.; Ebbesen, T. W. Channel Plasmon Subwavelength Waveguide Components Including Interferometers and Ring Resonators. *Nature* **2006**, *440*, 508−511.
(22) Kress, S. J. P.; Richner, P.; Jayanti, S. V.; Galliker, P.; Kim, D. K.; Poulikakos, D.; Norris, D. J. Near-Field Light Design with Colloidal Quantum Dots for Photonics and Plasmonics. *Nano Lett.* **2014**, *14*, 5827−5833.
(23) Kress, S. J. P.; Antolinez, F. V.; Richner, P.; Jayanti, S. V.; Kim, D. K.; Prins, F.; Riedinger, A.; Fischer, M. P. C.; Meyer, S.; McPeak, K. M.; Poulikakos, D.; Norris, D. J. Wedge Waveguides and Resonators for Quantum Plasmonics. *Nano Lett.* **2015**, *15*, 6267−6275.
(24) Quinten, M.; Leitner, A.; Krenn, J. R.; Aussenegg, F. R. Electromagnetic Energy Transport *via* Linear Chains of Silver Nanoparticles. *Opt. Lett.* **1998**, *23*, 1331.
(25) Brongersma, M. L.; Hartman, J. W.; Atwater, H. A. Electromagnetic Energy Transfer and Switching in Nanoparticle Chain Arrays below the Diffraction Limit. *Phys. Rev. B: Condens. Matter Mater. Phys.* **2000**, *62*, R16356−R16359.
(26) Maier, S. A.; Kik, P. G.; Atwater, H. A.; Meltzer, S.; Harel, E.; Koel, B. E.; Requicha, A. A. G. Local Detection of Electromagnetic Energy Transport below the Diffraction Limit in Metal Nanoparticle Plasmon Waveguides. *Nat. Mater.* **2003**, *2*, 229−232.
(27) de Torres, J.; Ferrand, P.; Colas des Francs, G.; Wenger, J. Coupling Emitters and Silver Nanowires to Achieve Long-Range Plasmon-Mediated Fluorescence Energy Transfer. *ACS Nano* **2016**, *10*, 3968−3976.
(28) Bouchet, D.; Lhuillier, E.; Ithurria, S.; Gulinatti, A.; Rech, I.; Carminati, R.; De Wilde, Y.; Krachmalnicoff, V. Correlated Blinking of Fluorescent Emitters Mediated by Single Plasmons. *Phys. Rev. A: At., Mol., Opt. Phys.* **2017**, *95*, No. 033828.
(29) Oulton, R. F.; Bartal, G.; Pile, D. F. P.; Zhang, X. Confinement and Propagation Characteristics of Subwavelength Plasmonic Modes. *New J. Phys.* **2008**, *10*, 105018.
(30) Synge, E. H., III A Microscopic Method. *London, Edinburgh, Dublin Philos. Mag. J. Sci.* **1931**, *11*, 65−80.
(31) Babayan, Y.; McMahon, J. M.; Li, S.; Gray, S. K.; Schatz, G. C.; Odom, T. W. Confining Standing Waves in Optical Corrals. *ACS Nano* **2009**, *3*, 615−620.
(32) Schoen, D. T.; Coenen, T.; García De Abajo, F. J.; Brongersma, M. L.; Polman, A. The Planar Parabolic Optical Antenna. *Nano Lett.* **2013**, *13*, 188−193.
(33) Drezet, A.; Stepanov, A. L.; Ditlbacher, H.; Hohenau, A.; Steinberger, B.; Aussenegg, F. R.; Leitner, A.; Krenn, J. R. Surface Plasmon Propagation in an Elliptical Corral. *Appl. Phys. Lett.* **2005**, *86*, 074104.
(34) Aeschlimann, M.; Brixner, T.; Cinchetti, M.; Frisch, B.; Hecht, B.; Hensen, M.; Huber, B.; Kramer, C.; Krauss, E.; Loeber, T. H.; Pfeiffer, W.; Piecuch, M.; Thielen, P. Cavity-Assisted Ultrafast Long-Range Periodic Energy Transfer between Plasmonic Nanoantennas. *Light: Sci. Appl.* **2017**, *6*, No. e17111.
(35) Hensen, M.; Heilpern, T.; Gray, S. K.; Pfeiffer, W. Strong Coupling and Entanglement of Quantum Emitters Embedded in a Nanoantenna-Enhanced Plasmonic Cavity. *ACS Photonics* **2018**, *5*, 240−248.
(36) Nagpal, P.; Lindquist, N. C.; Oh, S. H.; Norris, D. J. Ultrasmooth Patterned Metals for Plasmonics and Metamaterials. *Science* **2009**, *325*, 594−597.
(37) McPeak, K. M.; Jayanti, S. V.; Kress, S. J. P.; Meyer, S.; Iotti, S.; Rossinelli, A.; Norris, D. J. Plasmonic Films Can Easily Be Better: Rules and Recipes. *ACS Photonics* **2015**, *2*, 326−333.
(38) Dorn, R.; Quabis, S.; Leuchs, G. Sharper Focus for a Radially Polarized Light Beam. *Phys. Rev. Lett.* **2003**, *91*, 233901.
(39) Akimov, A. V.; Mukherjee, A.; Yu, C. L.; Chang, D. E.; Zibrov, A. S.; Hemmer, P. R.; Park, H.; Lukin, M. D. Generation of Single Optical Plasmons in Metallic Nanowires Coupled to Quantum Dots. *Nature* **2007**, *450*, 402−406.
(40) Galliker, P.; Schneider, J.; Eghlidi, H.; Kress, S.; Sandoghdar, V.; Poulikakos, D. Direct Printing of Nanostructures by Electrostatic Autofocussing of Ink Nanodroplets. *Nat. Commun.* **2012**, *3*, 890.
(41) Xiong, X.; Zou, C.-L.; Ren, X.-F.; Liu, A.-P.; Ye, Y.-X.; Sun, F.-W.; Guo, G.-C. Silver Nanowires for Photonics Applications. *Laser Photonics Rev.* **2013**, *7*, 901−919.

DOI: 10.1021/acsnano.9b03201
ACS Nano 2019, 13, 9048−9056

(42) Brucoli, G.; Martín-Moreno, L. Effect of Defect Depth on Surface Plasmon Scattering by Subwavelength Surface Defects. *Phys. Rev. B: Condens. Matter Mater. Phys.* **2011**, *83*, No. 075433.
(43) Klimov, V. I. *Nanocrystal Quantum Dots*; CRC Press: Boca Raton, FL, 2010; pp 2−13.
(44) Rabouw, F. T.; de Mello Donega, C. Excited-State Dynamics in Colloidal Semiconductor Nanocrystals. *Topics in Current Chemistry*; Springer: Cham, Switzerland, 2016; Vol. *374*, pp 1−30.
(45) Kagan, C. R.; Murray, C. B.; Bawendi, M. G. Long-Range Resonance Transfer of Electronic Excitations in Close-Packed CdSe Quantum-Dot Solids. *Phys. Rev. B: Condens. Matter Mater. Phys.* **1996**, *54*, 8633−8643.
(46) Crooker, S. A.; Hollingsworth, J. A.; Tretiak, S.; Klimov, V. I. Spectrally Resolved Dynamics of Energy Transfer in Quantum-Dot Assemblies: Towards Engineered Energy Flows in Artificial Materials. *Phys. Rev. Lett.* **2002**, *89*, 186802.
(47) Akselrod, G. M.; Prins, F.; Poulikakos, L. V.; Lee, E. M. Y.; Weidman, M. C.; Mork, A. J.; Willard, A. P.; Bulović, V.; Tisdale, W. A. Subdiffusive Exciton Transport in Quantum Dot Solids. *Nano Lett.* **2014**, *14*, 3556−3562.
(48) Ford, G. W.; Weber, W. H. Electromagnetic Interactions of Molecules With Metal Surfaces. *Phys. Rep.* **1984**, *113*, 195−287.
(49) Andersen, M. L.; Stobbe, S.; Sørensen, A. S.; Lodahl, P. Strongly Modified Plasmon-Matter Interaction with Mesoscopic Quantum Emitters. *Nat. Phys.* **2011**, *7*, 215−218.
(50) Prins, F.; Kim, D. K.; Cui, J.; De Leo, E.; Spiegel, L. L.; McPeak, K. M.; Norris, D. J. Direct Patterning of Colloidal Quantum-Dot Thin Films for Enhanced and Spectrally Selective Out-Coupling of Emission. *Nano Lett.* **2017**, *17*, 1319−1325.

DOI: 10.1021/acsnano.9b03201
ACS Nano 2019, 13, 9048−9056